Soft Matter

RSC Publishing

PAPER

View Article Online
View Journal | View Issue

Detachment and fracture of cellular aggregates†

Cite this: *Soft Matter*, 2013, **9**, 2282

David Gonzalez-Rodriguez,‡*[a] Louise Bonnemay,§[a] Jens Elgeti,[b] Sylvie Dufour,[c] Damien Cuvelier[a] and Françoise Brochard-Wyart[a]

Received 16th July 2012
Accepted 11th December 2012

DOI: 10.1039/c2sm26648b

www.rsc.org/softmatter

The dynamics of cellular adhesion and deadhesion, which play key roles in many cellular processes, have most often been studied at the scale of single bonds or single cells. However, multicellular adhesion and deadhesion are also central processes in tissue mechanics, morphogenesis, and pathophysiology, where collective tissue phenomena may introduce additional effects that are absent at the single-cell level. In this paper we present experiments on the adhesion of cellular aggregates and a laboratory model system to study tissue mechanics. We introduce a technique to measure the forces and energies involved in the detachment of an aggregate from a substrate (which can be viewed as a *cellular tack* assay) and in the fracture between two partially fused aggregates, as a function of the adhesion time, the pulling speed, and the cadherin density at the cell surface. We develop a model based on polymer physics to interpret the observations. We identify a significant contribution to the adhesion energy of viscous dissipation mechanisms present at the tissue scale that are absent at the single-cell level, as well as a significant effect of the speed at which the separation force is applied.

1 Introduction

Cell adhesion and deadhesion play key roles in several major cellular processes, such as proliferation, migration, differentiation, and death.[1] For this reason, the study of cell adhesion is a central topic in cell biology and biophysics. Many previous biophysical investigations of the dynamics of cell adhesion and deadhesion have considered the scale of a single molecular bond[2–6] or of a single cell.[7–11] However, in many relevant biological configurations, cell adhesion and detachment are multicellular processes where collective cell phenomena at the tissue scale may play important roles. There are many examples of multicellular and tissue deadhesion phenomena. For example, in morphogenesis, multicellular adhesion and deadhesion play a key role in tissue separation[12,13] or in the segregation of a continuous tissue into different units, such as in the formation of somites in vertebrates from the presomite mesoderm.[14] Multicellular adhesion and deadhesion are also important phenomena in pathophysiology, such as in the embolism-inducing detachment of thrombi[15] or in collective detachment and migration modes of cancer metastases.[16] Such multicellular adhesion phenomena may involve collective processes that are not fully captured by investigations at the single-cell level.

Cellular aggregates are a convenient experimental tool to study the biophysical properties of multicellular structures and tissues. In this context, cellular aggregates are typically spheroidal structures of a few hundred micrometers diameter formed by the aggregation and attachment of a few thousands of cells. They have previously been used to investigate tissue rheology,[17,18] showing that multicellular structures can be characterized as viscoelastic fluids with a surface tension[19] plus an active contractile response.[20] A review of experimental techniques used to characterize aggregate rheology can be found in ref. 21. According to the viscoelastic description,[19] cellular aggregates exhibit a short-time elastic behavior characterized by an elastic modulus E_t, and a long-time viscous behavior characterized by a dynamic viscosity η_t, with the viscoelastic time $\tau_t \equiv \eta_t/E_t$ being the characteristic time scale for transition from elastic to viscous behavior. Using cellular aggregates, the theoretical framework of soft matter physics has been applied to gain insight into collective tissue behaviors, such as spreading[22] or dewetting.[23] In cellular aggregates as well as in tissues,

[a]*Institut Curie, Centre National de la Recherche Scientifique, Unité Mixte de Recherche 168, and Université Paris 6, 75248 Paris, France. E-mail: davidgr@alum.mit.edu*

[b]*Forschungszentrum Jülich, 52425 Jülich, Germany*

[c]*Institut Curie, Centre National de la Recherche Scientifique, Unité Mixte de Recherche 144, 75248 Paris, France*

† Electronic supplementary information (ESI) available. Movie 1: Example of a detachment experiment. The left plate is displaced towards the left at a constant pulling speed v = 0.2 μm/s. The deflection of the cantilever on the right side indicates the applied force. The movie is speeded up. The elapsed time is displayed on the movie with a total recording time of 22 minutes and 30 seconds. The scale bar corresponds to 100 μm. Movie 2: Example of a fracture experiment. The left plate is displaced towards the left at a constant pulling speed v = 0.05 μm/s. The deflection of the cantilever on the right side indicates the applied force. The movie is speeded up. The elapsed time is displayed on the movie with a total recording time of one hour and 40 minutes. The scale bar corresponds to 100 μm. See DOI: 10.1039/c2sm26648b

‡ Present address: Laboratoire d'Hydrodynamique, Ecole Polytechnique, 91128 Palaiseau, France.

§ Present address: Département de Chimie, Ecole Normale Supérieure, 75230 Paris, France.

cadherins are a crucial mediator of intercellular adhesion. Cadherins are transmembrane proteins which form bonds with other cadherin molecules in neighboring cells. Adhesion to a substrate (or to the extracellular matrix) is mediated by a variety of proteins, among which the integrin family plays a major role.

Polymer physics provides valuable insights into cell adhesion.[24] A fundamental assay to measure polymer adhesion is called tack.[25–27] In this assay, a flat probe is brought into contact with a thin layer of the polymer adhesive deposited on a rigid substrate. The probe is then pulled away while measuring the applied force, which allows the adhesive properties of the polymer adhesive to be quantified.

This paper applies soft matter and polymer physics concepts to understand multicellular adhesion and deadhesion in the context of tissue mechanics. We present an experimental study of the detachment of a cellular aggregate from a rigid, adhesive surface (a cellular analogue of the tack assay), and of the fracture between two partially fused aggregates. We measure the forces and energies for detachment and fracture as a function of the contact time, the pulling velocity, and the cadherin expression level. The two series of experiments allow us to gain insight into the multicellular adhesion to a substrate or the extracellular matrix (detachment experiment) as well as into the cadherin-mediated intercellular tissue adhesion (fracture experiment). We interpret our observations by means of an analytical model that applies and extends a previous theoretical model of polymer adhesion.[28–30] By combining experiments and theoretical modeling, we identify the important contribution of viscous energy dissipation mechanisms present at the tissue scale that are absent both at the single-cell level and in polymeric adhesives. We also identify the significant effect of the speed at which the force is applied on the resistance of the aggregate to fracture.

2 Experimental

2.1 Preparation of cellular aggregates

We prepare aggregates from murine sarcoma (S180) cell lines transfected to express different densities of E-cadherin molecules at their surface.[9] We use two different cell lines called LCAM, which expresses the highest E-cadherin level, and E48, which expresses 48% of the cadherin level of LCAM. Cells are cultured under a 5% CO_2 atmosphere in a culture medium consisting of Dulbecco's Modified Eagle Medium (DMEM) enriched with 10% calf serum, 1% glutamine, and 1% penicillin/streptomycin. Confluent cells are detached using trypsin/EDTA and resuspended in 5 ml of CO_2-equilibrated medium, at a concentration of 4×10^5 cells per ml. To form the aggregates, the suspension is transferred into a 25 ml Erlenmeyer flask, which is placed in an orbital shaker at 75 rpm at 37 °C for 18–24 hours. The Erlenmeyer flasks were precoated with a solution of 2% dimethylchlorosilane in chloroform to prevent cell adhesion to the surface. This technique, similar to that of Ryan *et al.*,[31] produces spherical aggregates of variable diameters up to 500 μm. The LCAM aggregates used in the experiments reported here had a mean diameter and standard deviation of 212 ± 21 μm, and E48 aggregates had 190 ± 79 μm.

2.2 Experimental setup

Fig. 1(a) shows a sketch of the experimental setup for the detachment experiment. The experiment is performed in a plastic Petri dish that has been partially filled with PDMS to reduce its internal volume in order to facilitate heating. The Petri dish is placed on an Axiovert 200 inverted microscope (Zeiss) equipped with a 10× objective lens. The Petri dish is filled with a CO_2-independent medium (Invitrogen, ref. 18045) and, once the setup is ready, the surface is sealed with a layer of light mineral oil to avoid evaporation. The chamber is heated by means of a heating stage (Warner Instruments). The temperature is monitored with a thermocouple, and the heating stage setting is adjusted in order to keep the inside temperature between 35 and 37 °C. A 1 mm wide, 75 μm thick glass slide cut to a length of approximately 50 mm is held fixed at one end and used as a cantilever beam to measure forces. The cantilever has been calibrated using a 0.1 mg precision scale, yielding a bending rigidity of the cantilever $EI = 3.2$ μN m^2, which corresponds to a typical cantilever stiffness of $k = 3EI/L^3 \approx 0.08$ N m^{-1}, where L is the distance from the clamping point to the point of application of the force (thus slightly shorter than the total length). Note that the value of k is determined for each experiment by measuring L, the distance from the cantilever clamping point to the point of attachment of the aggregate. The cantilever is rendered adhesive to the cells by coating it with a 0.1 g l^{-1} fibronectin (Sigma-Aldrich) in PBS solution. By means of a micropipette, a cellular aggregate is slightly pressed against the glass slide for a few minutes to attach it. Then, a fibronectin-coated glass plate, parallel to the glass cantilever, is brought into contact with the aggregate and kept in contact with zero force for a controlled attachment time t_c. Unlike the glass cantilever, the glass plate is very short and thus is virtually undeformable. Its position is controlled with a M-110.1DG piezoelectric unit driven by a Mercury C-863 DC motor controller (PI Instruments). The piezoelectric unit can move the plate at a constant speed v between 6.9×10^{-2} and 100 μm s^{-1}. After the attachment time t_c, the piezoelectric unit starts moving at a constant velocity of v (the instant when motion starts is taken as $t = 0$) until the aggregate detaches from the glass plate ($t = t_{end}$). The complete deformation and detachment process is recorded with a Luca R CCD camera (Andor). Snapshots of a detachment experiment taken at the beginning of the pulling, right before detachment, and right after detachment are shown in Fig. 1(c)–(e), respectively (see also Movie 1†). Fig. 1(d) and Movie 1† show that cell deformation is most pronounced in the neck region where detachment will occur, where cells become strained by about 100% compared to an average strain in the aggregate body of about 40%. This larger strain is indicative of a stress concentration in the detachment neck.

Fig. 1(b) shows a sketch of the experimental setup for the fracture experiment. The setup is very similar to that of the detachment experiment. In this case, one cellular aggregate is attached to the glass cantilever and another aggregate to the glass plate. The aggregates are left to attach to the plates for a long enough time so that they do not detach from the plates during the experiment. Then, the two aggregates are brought into contact and left to partially fuse with one another in the absence of external forces for a time t_c. After this fusing time t_c, the

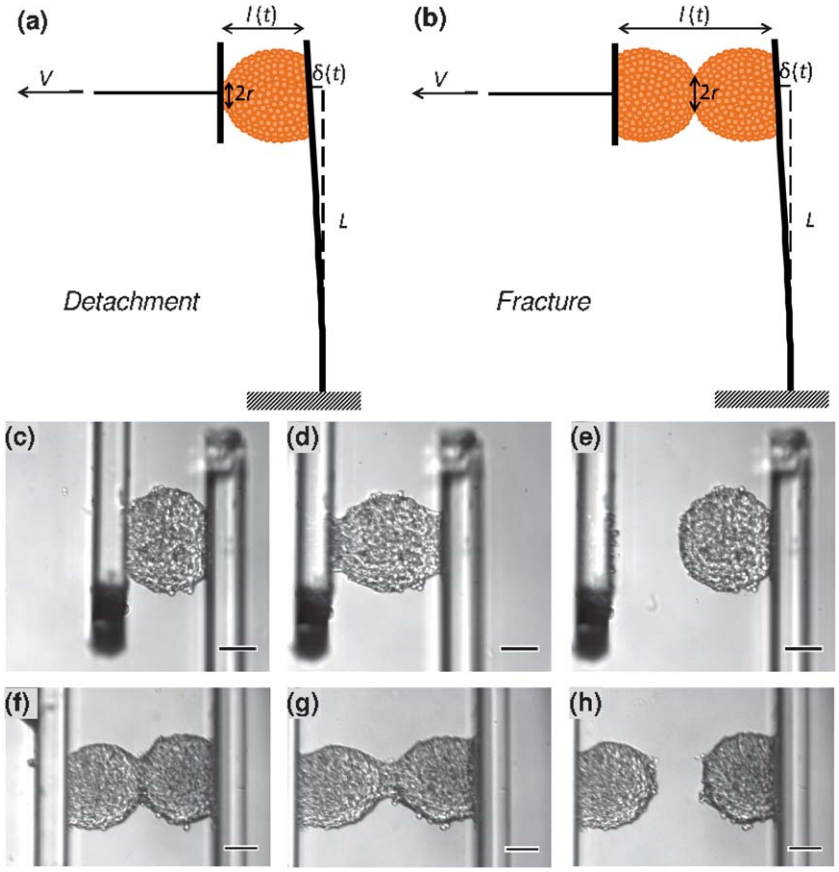

Fig. 1 Experimental setup. (a) Detachment experiment. The left plate is pulled at a velocity v until it detaches from the aggregate. The deflection of the cantilever on the right side indicates the applied force. (b) Fracture experiment. Two partially fused aggregates are pulled apart by the motion of the left plate. Sequence of images of the detachment experiment for a pulling speed $v = 0.2$ μm s^{-1} (see also Movie 1†): (c) zero applied force at the beginning of the experiment, (d) stretched aggregate right before detachment, (e) aggregate right after detachment. (f–h) Analogous sequence of images of the fracture experiment for a pulling speed $v = 0.05$ μm s^{-1} (see also Movie 2†). The scale bar corresponds to 100 μm.

piezoelectric motor starts pulling ($t = 0$) at a constant velocity v until the two aggregates break apart from each other ($t = t_{end}$). Snapshots of a fracture experiment taken at the beginning of the pulling, right before fracture, and right after fracture are shown in Fig. 1(f)–(h), respectively (see also Movie 2†).

Cell viability in aggregates was checked using the Trypan blue dye exclusion test.[32] At the end of a long experiment (10 h), Trypan blue is added to the experimental chamber to a final concentration of 20%, and the number of stained cells is compared to those in a freshly prepared aggregate. The number of dead cells present at the core of the aggregates is small and approximately the same in both cases, confirming that aggregates remain viable during the experiment.

The movie recorded during each experiment is analyzed using ImageJ. The image analysis yields the deflection of the cantilever as a function of time, $\delta(t)$, the distance between the two glass surfaces as a function of time, $l(t)$, and the width of the contact between the aggregate and the glass plate or between the two aggregates at the beginning of the pulling process, $2r$ (see Fig. 1(a) and (b)). The size of the contact remains approximately constant during most of the experiment, decreasing quickly only when detachment or fracture is approached. The effective force exerted by the glass cantilever on the aggregate is calculated as $F(t) = 3EI\delta(t)/L^3$, where $EI = 3.2$ μN m^2 is obtained from the cantilever calibration, and L is measured for each experiment and remains on the order of 50 mm. The instantaneous stress is obtained as $\sigma(t) = F(t)/(\pi r^2)$, where r is the initial radius of the contact. This expression neglects the reduction of the contact size in time, whose variation is indeed small for most of the experiments compared to the measurement error in determining the contact area from the side view. The instantaneous strain is computed as $\varepsilon(t) = (l(t) - l_0)/l_0$, where $l_0 = l(t = 0)$ is the separation between the two glass surfaces when pulling starts ($t = 0$). The maximum stress is $\sigma_{max} = \max_t\{\sigma(t)\}$. The deadhesion energy density G is calculated as

$$G = \int_{t=0}^{t=t_{end}} \sigma(t)\mathrm{d}l(t). \quad (1)$$

2.3 Experimental results

Fig. 2 illustrates the rheological response of a cell aggregate to pulling. It shows measurements corresponding to two specific fracture experiments with $t_c = 60$ min and $v = 5.0$ μm s^{-1} or $v = 0.02$ μm s^{-1}, using aggregates of the LCAM cell line. Fig. 2(a)

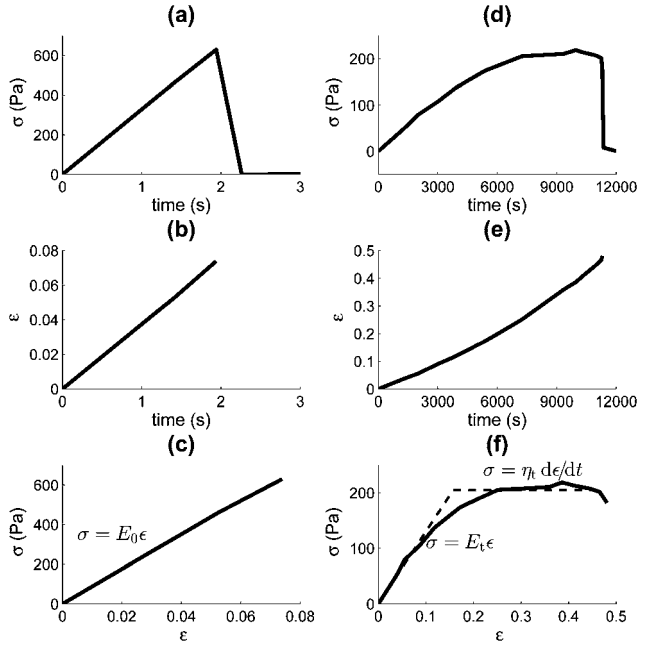

Fig. 2 Experimental results for two fracture experiments with contact time t_c = 60 min and pulling speeds v = 5.0 μm s^{-1} (a–c) or v = 0.02 μm s^{-1} (d–f). Data points are acquired every 0.5 s or every 30 s, respectively for the high and low pulling speeds. (a and d) Time evolution of the pulling stress σ deduced from the deflection of the cantilever. Fracture occurs at t_{end} = 2 s or t_{end} = 11 300 s, respectively. (b and e) Time evolution of the aggregate strain ε obtained from the experimental images. (c and f) Experimentally deduced stress–strain relationship (full line). In (c) the response is linear elastic with modulus $E_0 \approx$ 9000 Pa. In (f) the dashed line represents a viscoelastic interpretation of the experimental curve, with an elastic modulus $E_t \approx$ 1000 Pa and an apparent viscosity $\eta_t \approx 5 \times 10^6$ Pa s.

and (d) show the time evolution of the pulling stress σ deduced from the cantilever deflection, up to fracture, which occurs at $t = 2$ s and $t = 11\,300$ s, respectively. The fast pulling experiment (Fig. 2(a)) shows a purely elastic behavior, while in the slow pulling experiment (Fig. 2(d)) the stress increases linearly at short time (elastic regime) and becomes constant at long time (viscous regime). Fig. 2(b) and (e) show the time evolution of the strain ε. During most of the experiments ε increases linearly in time, corresponding to the imposed constant pulling velocity v. However, near fracture, the deformation rate speeds up slightly for the slow pulling experiment, due to large deformations localized near the fracture region. Fig. 2(c) and (f) show the stress–strain relationship, which can be characterized as elastic at short time and viscous at long time. Considering the results from all the LCAM fracture experiments at pulling speeds $v \leq$ 0.02 μm s^{-1} ($N_{exp} = 8$), we deduce an elastic modulus $E_t \approx 1000 \pm 300$ Pa, which corresponds to the slope of the stress–strain curves at low pulling speeds (Fig. 2(f)), and an apparent viscosity $\eta_t \approx 5 \times 10^6 \pm 3 \times 10^6$ Pa s, which is given by the ratio between σ and dε/dt in the long-time viscous region where σ is constant (Fig. 2(e) and (f)). The resulting estimate of the viscoelastic time, $\tau_t = \eta_t/E_t$, is of the order of one hour. These rheological values are consistent with those reported in micropipette aspiration experiments, where the deformed geometry is more precisely controlled and where a tissue viscoelastic time of 44 ± 7 min was obtained.[19] As expected, in contrast to the slow pulling experiments, fracture experiments at high pulling speeds (v > 1 μm s^{-1}) exhibit a purely elastic behavior, with a linear stress–strain relationship (Fig. 2(c)). Moreover, the very short time (<1 s) elastic modulus deduced from the initial slope of the stress–strain relationship in the fast pulling experiments ($N_{exp} = 8$) is $E_0 \approx 9000 \pm 2000$ Pa, about 10 times larger than E_t, the elastic modulus measured over a time scale of minutes. It is also noted that, in some of the low velocity experiments, aggregate pulsation was observed (see Movie 2†), which appears to be a manifestation of the previously described phenomenon of aggregate shivering under stretch.[20] Aggregate detachment at high and low pulling speeds exhibit similar rheological responses to the fracture experiments (Fig. S1 in the ESI†).

Fig. 3 shows the maximum stress σ_{max} at detachment or fracture (Fig. 3(a)) and the deadhesion energy density G (Fig. 3(b)) as a function of the pulling speed v for both the detachment and fracture experiments with the LCAM (reference E-cadherin density) and E48 (48% of the reference density) cell lines. Both the maximum stress and the deadhesion energy are normalized by the contact area before fracture, πr^2, with r being the radius of the contact area, which remains approximately constant until shortly before fracture or detachment occurs (Fig. 1(a), (b), (d) and (g)). The contact time is fixed at $t_c = 60$ min. In the LCAM fracture experiments (red squares), both σ_{max} and G are low at low v and increase to reach a maximum at around $v \approx 0.03$ μm s^{-1}. This maximum is followed by a decrease of both σ_{max} and G, which reach a minimum at around

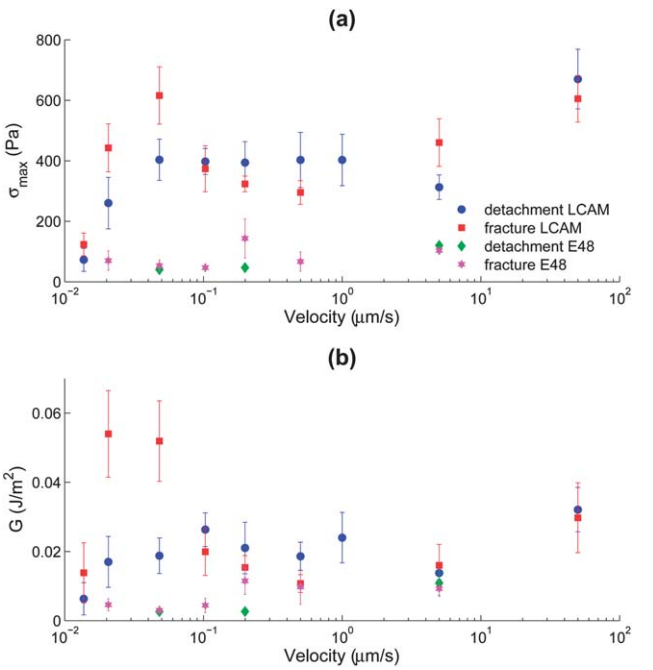

Fig. 3 (a) Maximum stress at detachment or fracture and (b) deadhesion energy density as a function of the pulling speed v for a fixed contact time t_c = 60 min. Blue circles: detachment experiments with the LCAM cell line (number of experiments, from lower to higher v: N = 4, 3, 3, 4, 5, 4, 4, 4, 4); red squares: fracture experiments with the LCAM cell line (N = 3, 4, 7, 3, 9, 6, 4, 4); green diamonds: detachment experiments with the E48 cell line (N = 3, 3, 3); magenta hexagrams: fracture experiments with the E48 cell line (N = 3, 3, 3). The error bars correspond to standard errors.

$v \approx 0.5$ μm s^{-1}, followed by a new increase of both quantities at very high pulling velocity. The LCAM detachment experiments (blue circles) show values of σ_{max} and G comparable to the fracture experiments and also a comparable dependence on v, albeit less pronounced; most notably, the existence of a maximum at moderate pulling velocities is unclear. The minimum deadhesion energy density in LCAM fracture is $G_0 \approx 0.01$ J m^{-2}. The fracture and detachment experiments with the E48 cell line (magenta hexagrams and green diamonds, respectively) yield stresses and adhesion energies that are about 4 times smaller than those of the LCAM ($G_{0,E48} \approx 0.002$ J m^{-2}). This decrease of maximum stresses and adhesion energies with decreasing E-cadherin density is consistent with previous studies, which showed that the force required to separate two cells was proportional to the square of their E-cadherin surface density.[9] The observed velocity dependence of σ_{max} and G for E48 cells (magnified image shown in Fig. S2 in the ESI†) is comparable to the spread in the data arising from population variability and limited precision of our experimental apparatus. Thus, our measurements do not allow us to characterize the velocity dependence for the E48 cell line.

Fig. 4 shows the maximum stress σ_{max} at detachment or fracture (Fig. 4(a)) and the deadhesion energy G (Fig. 4(b)) as a function of the contact time t_c for both the detachment and fracture experiments with the LCAM cell line. The pulling speed is fixed at $v = 0.20$ μm s^{-1}. In the fracture experiments (red squares), the adhesion strength increases monotonically with the contact time, reflecting the progressive fusion of the two aggregates in contact. The evolution of the shape prior to pulling reflects the dynamics of aggregate spreading.[22] A remarkable feature of the detachment data shown in Fig. 4 (blue circles) is that both σ_{max} and G increase up to a maximum for a contact time $t_c \approx 45$–60 min, and then they decrease. For $t_c < 60$ min, the stress and deadhesion energy are larger for detachment than for fracture, while for $t_c > 60$ min they become slightly smaller for detachment. To explain this transition, an insightful observation is that in detachment experiments with short t_c the detachment is adhesive and no cells are left on the plate, suggesting that detachment involves the cell–substrate integrin bonds. For long t_c the detachment becomes cohesive, with a layer of cells left on the plate after detachment, indicating that detachment involves the cell–cell cadherin bonds. This transition is attributed to the aggregate spreading process, whose characteristic evolution time is of the order of one hour.[22] At short times, the aggregate has a nearly spherical shape, which causes a stress concentration and thus detachment at the cell–substrate contact. The increase of adhesion strength over the first 30 minutes is due to the slow maturation of integrin–fibronectin bonds.[33] At long times, of the order of one hour, aggregate spreading has formed a neck between the aggregate core and the film of spreading cells, which causes a local concentration of stresses at the neck, favoring cell–cell detachment at this location. Thus, for the long times ($t_c > 60$ min), both detachment and fracture correspond to the breakup of cell–cell bonds. The slightly larger G at long time in the fracture experiments may be due to the larger size of the system (two aggregates *versus* one aggregate in the detachment experiment), which results in a larger viscous energy dissipation.

Fig. 5 shows the maximum strain ε_{max} at detachment or fracture as a function of the pulling speed v for both the detachment and fracture experiments with the LCAM cell line. The contact time is fixed at $t_c = 60$ min. Since the fracture of elastic materials is characterized by a constant maximum deformation independent of the pulling velocity,[34] in this figure a material that was dominantly elastic would be represented by a horizontal line. The figure shows that, for the detachment experiments, the maximum strain is approximately constant, since the variations of maximum strain with velocity are

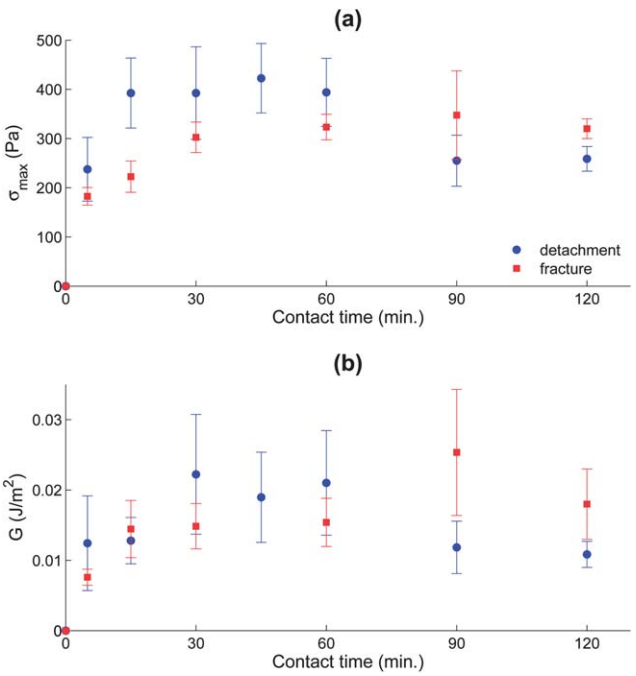

Fig. 4 (a) Maximum stress at detachment or fracture and (b) deadhesion energy as a function of the contact time t_c for a fixed pulling speed $v = 0.20$ μm s^{-1}. Blue circles: detachment experiments with the LCAM cell line ($N = 4, 4, 4, 4, 5, 4, 4$); red squares: fracture experiments with the LCAM cell line ($N = 4, 4, 4, 9, 4, 2$). The error bars correspond to standard errors.

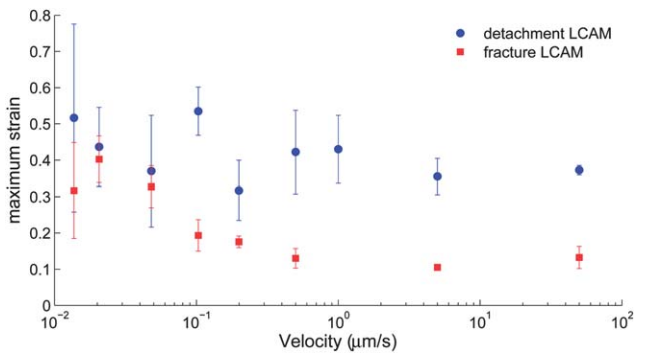

Fig. 5 Maximum strain at detachment or fracture as a function of the pulling speed v for a fixed contact time $t_c = 60$ min. Blue circles: detachment experiments with the LCAM cell line ($N = 3, 3, 3, 4, 7, 4, 4, 4, 4$); red squares: fracture experiments with the LCAM cell line ($N = 3, 4, 7, 3, 9, 6, 4, 4$). The error bars correspond to standard errors.

comparable to the error bars (the experimental dispersion for a given velocity). This suggests that aggregate detachment can be modeled by the detachment of an elastic material. In contrast, in the fracture experiments, an elastic behavior is only an accurate model at large speeds, while viscous dissipation effects play an important role at low pulling speeds, as indicated in Fig. 5 by the increase of maximum strain at low velocity.

3 Theoretical model

As discussed by P.-G. de Gennes,[35] adhesion is most appropriately characterized in terms of deadhesion energy G and not in terms of the critical stress for separation σ_{max}, since the stress distribution is highly dependent on the geometry of the adhesive. Thus, here we focus on understanding the observed dependence of the deadhesion energy on the pulling velocity, $G(v)$, for the case of the LCAM cell line.

Interpretation of the detachment experiments is complex, since, as discussed above, adhesion is mediated by two types of molecular interactions (cadherin–cadherin and integrin–fibronectin) with very different dynamics. The experimental observations suggest that the deadhesion energy is relatively independent of the pulling velocity when compared to the fracture case (Fig. 4b), with an approximately constant value of $G \approx 0.01$–0.02 J m^{-2}. The less pronounced effect of the velocity in the detachment experiments compared to the fracture experiments can be partially explained by the smaller material thickness in the detachment experiments (thickness of one aggregate, *versus* two aggregates in the case of the fracture experiments), which will result in a smaller energy dissipation. A strong dependence of σ_{max} and G on the thickness has also been observed in detachment experiments of polymeric materials.[36] Moreover, the aggregate behavior during detachment seems well characterized by that of an elastic body (Fig. 5), with fracture occurring for a constant level of deformation of approximately $\varepsilon_{max} \approx 0.4$.

In contrast, fracture between two aggregates shows a marked dependence on the pulling speed, with a non-trivial shape of $G(v)$. From a biophysical perspective, however, aggregate fracture is a simpler problem than aggregate detachment, since adhesion in fracture is always mediated by cadherin–cadherin interactions. We thus propose a simple model to interpret the observed dependence on $G(v)$ based on a model originally developed by P.-G. de Gennes for the fracture of a polymer adhesive[28,29] and later extended by Saulnier *et al.*[30] This model for polymer detachment, which we will refer to as the *Modified de Gennes Model* (MdGM), expresses the deadhesion energy as a sum of two components,

$$G(v) = G_0 + G_v(v), \tag{2}$$

where $G_0 = G(v = 0)$ is the thermodynamic deadhesion energy at zero pulling velocity, and it represents local processes in the fracture region, while $G_v(v)$ is the viscous energy dissipation due to viscoelastic losses in the bulk of the adhesive. When studying thin polymer adhesives, the relevant velocity is the velocity of propagation of the crack. In the case of aggregate deadhesion, most of the viscous dissipation occurs by deformation of the aggregate body, and thus the relevant velocity is the velocity of deformation of the aggregate, determined by the plate speed v. The rheological behavior of the adhesive is characterized by the equation

$$\underline{\sigma} = \underline{\mu}\,\underline{\varepsilon} \tag{3}$$

where the underline indicates a complex quantity. $\underline{\sigma} \equiv \hat{\sigma} e^{i\omega t}$ and $\underline{\varepsilon} \equiv \hat{\varepsilon} e^{i\omega t}$ are respectively the complex stress and strain, with $\hat{\sigma}$ and $\hat{\varepsilon}$ being their moduli, t the time, and i the imaginary unit. ω is the frequency of solicitation, which scales as $\omega \approx v/\rho$, where v is the pulling velocity and ρ the radial distance to the fracture tip. $\underline{\mu} = \mu'(\omega) + i\mu''(\omega)$ is the complex modulus. The rate of energy dissipation per unit length of the fracture line is:[29]

$$T\dot{S} = \iint \mathrm{Re}\left[\frac{\underline{\sigma}\,\underline{\varepsilon}^*}{2}\right] \mathrm{d}x\mathrm{d}y, \tag{4}$$

where Re indicates the real part and * indicates the complex conjugate. Performing the integration and using the standard relationship from fracture mechanics $G_0 = K_I^2/\mu_\infty$, where K_I is the applied stress intensity factor that gives the stress distribution near the fracture tip and $\mu_\infty = E_0 + E_t$ is the effective elastic modulus of the material under fast loading (see Saulnier *et al.*[30] for details), the following relationship is obtained:[29,30]

$$\frac{G_v(v)}{G_0} \approx (E_0 + E_t) \int_{\omega_{min}}^{\omega_{max}} \frac{\mu''(\omega)}{\mu'(\omega)^2 + \mu''(\omega)^2} \frac{\mathrm{d}\omega}{\omega}. \tag{5}$$

The limits of integration are $\omega_{min} = v/R$ and $\omega_{max} = v/r$, where r is the radius of the contact zone (see Fig. 1) and R the radius of the adhesive (in our case, the radius of the cellular aggregate). It is noted that the predictions of our model depend only weakly on the values of these integration limits, whose choice is based on scaling arguments.[30]

Saulnier *et al.*[30] obtained an analytical solution of eqn (5) for a cross-linked polymer whose rheology is characterized by Zener's model (a spring in parallel to a subsystem formed by a spring and a damper in series). A cellular aggregate has been characterized by the slightly more complex rheological model proposed by Guevorkian *et al.*,[19] shown in Fig. 6(a). In this rheological model, the spring of constant E_0 represents the very short time elastic cell response observed both in micropipette aspiration and in the current experiments, where we have measured $E_0 \approx 9000 \pm 2000$ Pa. The spring of constant E_t represents the slower elastic response observed over a time scale of minutes, which is measured to be $E_t \approx 1000 \pm 300$ Pa, consistent with the value of 700 Pa reported by Guevorkian *et al.*[19] The damper of constant η_0 represents the cell viscosity, which is found in the literature to be $\eta_0 \approx 300$ Pa s.[37] The damper of constant η_t represents the apparent tissue viscosity, due to relative cell–cell motion and changes in cell neighbors allowed by the dynamic nature of cadherin bonds, and it is estimated from the current experiments to be $\eta_t \approx 5 \pm 3 \times 10^6$ Pa s. This second damper is an added feature to the simpler Zener's model, which was used to characterize polymer rheology in the MdGM.[30] The aggregate rheology is thus characterized by two time scales: the viscoelastic time scale

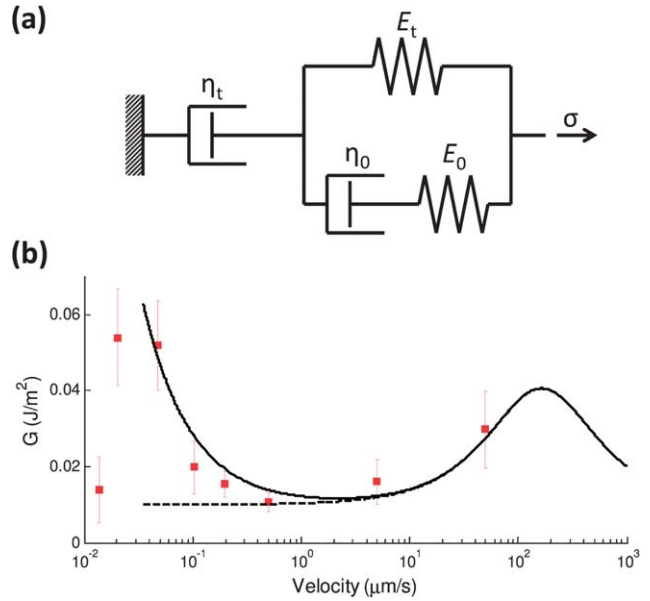

Fig. 6 (a) Viscoelastic model of the aggregate rheology,[19] consisting of two springs of elastic moduli E_0 and E_t and two dampers of viscosities η_0 and η_t. (b) Comparison between our model's prediction (full line) and experiments (red squares, N = 3, 4, 7, 3, 9, 6, 4, 4) of the deadhesion energy as a function of the pulling speed for a fixed contact time t_c = 60 min. The dashed line is the prediction of the MdGM for a cross-linked polymer.[30] The error bars correspond to standard errors of the measurements.

associated with the short-time elasticity, $\tau_0 \equiv \eta_0/E_0 \approx 0.3$ s, and the tissue viscoelastic time scale, $\tau_t \equiv \eta_t/E_t \approx 45$ min. The stress–strain relationship in the rheological model in Fig. 6(a) results from combining the constitutive equation of Zener's model[30] with that of the second damper in series to obtain:

$$\frac{E_t}{\eta_t}\sigma + \left(1 + \frac{\eta_0(E_0+E_t)}{\eta_t E_0}\right)\frac{\mathrm{d}\sigma}{\mathrm{d}t} + \frac{\eta_0}{E_0}\frac{\mathrm{d}^2\sigma}{\mathrm{d}t^2} = E_t\frac{\mathrm{d}\varepsilon}{\mathrm{d}t} + \eta_0\frac{E_0+E_t}{E_0}\frac{\mathrm{d}^2\varepsilon}{\mathrm{d}t^2}. \quad (6)$$

By introducing the complex variables $\underline{\sigma} = \hat{\sigma}e^{i\omega t}$ and $\underline{\varepsilon} = \hat{\varepsilon}e^{i\omega t}$ into the previous equation, an expression for the complex modulus $\underline{\mu} = \mu'(\omega) + i\mu''(\omega) = \underline{\sigma}/\underline{\varepsilon}$ is obtained:

$$\mu' = \frac{E_t\left[1 + \lambda(\tau_0\omega)^2\right]}{\Delta} \quad (7)$$

$$\mu'' = \frac{E_t}{\tau_0\omega\Delta}\left[\frac{\tau_0}{\tau_t} + (\tau_0\omega)^2\left(\frac{\lambda^2\tau_0}{\tau_t} + \lambda - 1\right)\right] \quad (8)$$

$$\Delta = 1 + \frac{2\tau_0}{\tau_t}(\lambda - 1) + \frac{\lambda^2{\tau_0}^2}{{\tau_t}^2} + (\tau_0\omega)^2 + \frac{1}{(\tau_t\omega)^2}, \quad (9)$$

where $\lambda \equiv (E_0 + E_t)/E_t \approx 10$. By introducing eqn (7) and (8) into eqn (5) we obtain an integral expression for G_v/G_0 that is easily evaluated numerically. The total deadhesion energy is then predicted as $G(v) = G_0(1 + G_0/G_v(v))$, where $G_0 \approx 0.01$ J m^{-2} is the only fitting parameter in the model, and its value is taken equal to the minimum deadhesion energy measured in the experiments. G_0 corresponds to the deadhesion energy when the elastic behavior dominates and viscous dissipation effects can be neglected. Accordingly, the fitted value of G_0 can correctly be estimated using Johsson–Kendall–Roberts's theory for the detachment of elastic solids,[38,39] which predicts a deadhesion energy of the order of $G_0 \approx RE_t \approx 0.01$ J m^{-2}.

Fig. 6(b) shows a comparison between $G(v)$ predicted by this model (solid line) and the experimental measurements (red squares). The model's prediction uses geometrical parameters based on the experimental configuration (r = 50 μm, R = 100 μm), rheological values deduced from the stress–strain curves and consistent with the literature (τ_0 = 0.3 s, τ_t = 45 min, λ = 10), and only one fitted parameter $G_0 = 0.01$ J m^{-2}. Fig. 6(b) also shows the predictions of the MdGM (dashed line), which does not account for tissue viscosity. According to our model's interpretation, the deadhesion energy $G(v)$ becomes significant for two specific ranges of pulling speeds. A local maximum of $G(v)$ occurs for a pulling speed $v \approx R/\tau_0$, at which the deadhesion energy is dominated by viscoelastic dissipation at the cellular scale. This region of the curve is analogous to the behavior of a cross-linked polymer, which can be represented by the Zener model. For cellular aggregates, there is another region of significant energy dissipation at a pulling speed $v \approx R/\tau_t$, at which the deadhesion energy is dominated by tissue viscoelastic dissipation. At this low pulling speed, the aggregate behavior can be represented by a Maxwell model consisting of a damper of viscosity η_t in series with a spring of elasticity E_t, and thus it behaves like an uncrosslinked polymer with G_v/G_0 increasing as $1/v$.[30] This large dissipation energies at velocities $v \approx R/\tau_t$ is a tissue-specific feature absent both in polymer fracture and in single-cell deadhesion. At intermediate speeds ($R/\tau_t \ll v \ll R/\tau_0$) viscous dissipation becomes small and the deadhesion energy is only due to local thermodynamic effects, $G \approx G_0$. At very low speeds ($v < R/\tau_t$), Fig. 6(b) shows a discrepancy between the experimental results and the aggregate behavior predicted by the Zener model. Indeed, based on the Zener model used in previous studies to successfully characterize the aggregate behavior,[19] we expected large deformations of the cellular aggregate at very low pulling velocities, with an elongated, thin thread of cells extending between the separating aggregates, similar to the cohesive failure seen in polymer tack at low velocities.[36] This phenomenon was however not observed. Instead, the detachment energy becomes small at very low pulling speeds. Since the low pulling experiments last for a few hours, this weakening could be due to biological changes in the cells due to the suboptimal conditions of the experimental chamber.

4 Conclusion

We have studied the detachment of a cellular aggregate from a fibronectin-coated plate, as well as the fracture between two partially fused aggregates. When subjected to a pulling force, aggregates behave viscoelastically, as previously described.[19] Analogous to the fracture of a polymer adhesive, the pulling speed has a significant influence on the deadhesion energy G for aggregate fracture. When the time scale of the experiment is close to the tissue viscoelastic time scale $\tau_t \approx \eta_t/E_t$, tissue viscoelastic dissipation increases the deadhesion energy up to a

value $G_{max} \approx 0.05$ J m^{-2}. This is a collective cell effect specific to tissues that would be absent in single cell–cell fracture. In addition, when the time scale of the experiment is close to the short-time cell viscoelastic response time, $\tau_0 \approx \eta_0/E_0$, the deadhesion energy is significantly increased by viscous dissipation in the cells. Far from these two time scales, viscous effects are negligible and only thermodynamic effects local to the fracture site contribute to the deadhesion energy, which reaches a minimum value, $G_{min} = G_0 \approx 0.01$ J m^{-2}. Such a fine-tuned dependence of the adhesion energy on the time scale of the imposed conformational change is a potentially important mechanism in morphogenesis, where the temporal modulation of the adhesion strength is crucial to allow cells to undergo relative motions or to remain cohesive. Indeed, an experimental setup conceptually similar to that of the fracture experiments presented here has previously been used to investigate spatio-temporal variations of the tensile properties of embryonic tissues.[40] Aggregate detachment is more complex than aggregate fracture, since at short times (t < 1 hour) detachment occurs at the integrin–fibronectin bonds, while for slower experiments (t > 1 hour) detachment occurs at the cadherin–cadherin bonds. This is attributed to the strengthening of integrin bonds in the latter case, due to the experiment duration becoming longer than the maturation time of integrin bonds.[33] The deadhesion energy G for detachment has a less clear dependence on the pulling speed than in the case of aggregate fracture. When a different cell line expressing half the E-cadherin density is used, the deadhesion energy in both the fracture and detachment experiments is significantly reduced (by a factor of about 4), which is consistent with previous results on the effect of E-cadherin expression on single-cell adhesion.[9] In conclusion, this study demonstrates the existence of collective tissue effects in multicellular adhesion, as well as the non-negligible effect of the pulling velocity on the tissue deadhesion energy.

Acknowledgements

We thank Christophe Clanet for insightful discussions, Stéphane Douezan for valuable suggestions and help with the experimental setup, and Julien Husson for helpful comments on the manuscript. D.G.-R. was funded by Fondation Pierre-Gilles de Gennes.

References

1 J.-P. Thiery, *C. R. Phys.*, 2003, **4**, 289–304.
2 E. Evans and K. Ritchie, *Biophys. J.*, 1997, **72**, 1541–1555.
3 R. Merkel, P. Nassoy, A. Leung, K. Ritchie and E. Evans, *Nature*, 1999, **397**, 50–53.
4 D. F. Tees, R. E. Waugh and D. A. Hammer, *Biophys. J.*, 2001, **80**, 668–682.
5 G. Hummer and A. Szabo, *Biophys. J.*, 2003, **85**, 5–15.
6 F. Pincet and J. Husson, *Biophys. J.*, 2005, **89**, 4373–4381.
7 E. Evans, D. Berk, A. Leung and N. Mohandas, *Biophys. J.*, 1991, **59**, 849–860.
8 S. Pierrat, F. Brochard-Wyart and P. Nassoy, *Biophys. J.*, 2004, **87**, 2855–2869.
9 Y.-S. Chu, W. A. Thomas, O. Eder, F. Pincet, E. Perez, J.-P. Thiery and S. Dufour, *J. Cell Biol.*, 2004, **167**, 1183–1194.
10 Y.-S. Chu, S. Dufour, J.-P. Thiery, E. Perez and F. Pincet, *Phys. Rev. Lett.*, 2005, **94**, 028102.
11 M.-J. Colbert, F. Brochard-Wyart, C. Fradin and K. Dalnoki-Veress, *Biophys. J.*, 2010, **99**, 3555–3562.
12 J.-P. Thiery, J.-L. Duband, U. Rutishauser and G. M. Edelman, *Proc. Natl. Acad. Sci. U. S. A.*, 1982, **79**, 6737–6741.
13 M. Takeichi, *Development*, 1988, **102**, 639–655.
14 J.-L. Duband, S. Dufour, K. Hatta, M. Takeichi, G. M. Edelman and J.-P. Thiery, *J. Cell Biol.*, 1987, **104**, 1361–1374.
15 D. M. Wootton and D. N. Ku, *Annu. Rev. Biomed. Eng.*, 1999, **1**, 299–329.
16 T. S. Deisboeck and I. D. Couzin, *BioEssays*, 2009, **31**, 190–197.
17 R. A. Foty, G. Forgacs, C. M. Pfleger and M. S. Steinberg, *Phys. Rev. Lett.*, 1994, **72**, 2298–2301.
18 A. Mgharbel, H. Delanoë-Ayari and J.-P. Rieu, *HFSP J.*, 2009, **3**, 213–221.
19 K. Guevorkian, M.-J. Colbert, M. Durth, S. Dufour and F. Brochard-Wyart, *Phys. Rev. Lett.*, 2010, **104**, 218101.
20 K. Guevorkian, D. Gonzalez-Rodriguez, C. Carlier, S. Dufour and F. Brochard-Wyart, *Proc. Natl. Acad. Sci. U. S. A.*, 2011, **108**, 13387–13392.
21 D. Gonzalez-Rodriguez, K. Guevorkian, S. Douezan and F. Brochard-Wyart, *Science*, 2012, **338**, 910–917.
22 S. Douezan, K. Guevorkian, R. Naouar, S. Dufour, D. Cuvelier and F. Brochard-Wyart, *Proc. Natl. Acad. Sci. U. S. A.*, 2011, **108**, 7315–7320.
23 S. Douezan and F. Brochard-Wyart, *Soft Matter*, 2012, **8**, 784–788.
24 P. Nassoy, in *P.-G. de Gennes' Impact in Science – Soft Matter and Biophysics (Volume II)*, ed. J. Bok, J. Prost and F. Brochard-Wyart, World Scientific, 2009, ch. An approach to cell adhesion inspired from polymer physics, pp. 127–138.
25 A. Zosel, *Colloid Polym. Sci.*, 1985, **263**, 541–553.
26 C. Creton and P. Fabre, in *Adhesion Science Science and Engineering, Vol. I: The Mechanics of Adhesion*, ed. D. A. Dillard and A. V. Pocius, Elsevier, 2002, ch. Tack, pp. 535–576.
27 C. Gay, *Integr. Comp. Biol.*, 2002, **42**, 1123–1126.
28 P.-G. de Gennes, *Acad. Sci., Paris, C. R.*, 1988, **307**, 1949–1953.
29 P.-G. de Gennes, *Langmuir*, 1996, **12**, 4492–4496.
30 F. Saulnier, T. Ondarçuhu, A. Aradian and E. Raphaël, *Macromolecules*, 2004, **37**, 1067–1075.
31 P. L. Ryan, R. A. Foty, J. Kohn and M. S. Steinberg, *Proc. Natl. Acad. Sci. U. S. A.*, 2001, **98**, 4323–4327.
32 H. Shapiro, *Practical Flow Cytometry*, John Wiley & Sons, 1988.
33 P. Roca-Cusachs, N. C. Gauthler, A. del Rio and M. P. Sheetz, *Proc. Natl. Acad. Sci. U. S. A.*, 2009, **106**, 16245–16250.
34 K. L. Johnson, *Contact Mechanics*, Cambridge University Press, 1985.

35 P.-G. de Gennes, in *Studying Cell Adhesion*, ed. P. Bongrand, Springer Verlag, 1995, ch. Preface.
36 T. Ondarçuhu, *J. Phys. II*, 1997, **7**, 1893–1916.
37 D. Cuvelier, M. Théry, Y.-S. Chu, S. Dufour, J.-P. Thiéry, M. Bornens, P. Nassoy and L. Mahadevan, *Curr. Biol.*, 2007, **17**, 694–699.
38 K. L. Johnson, K. Kendall and A. D. Roberts, *Proc. R. Soc. London, Ser. A*, 1971, **324**, 301–313.
39 H. Gérardin, A. Burdeau, A. Buguin and F. Brochard-Wyart, *Langmuir*, 2007, **23**, 9704–9712.
40 C. Wiebe and G. W. Brodland, *J. Biomech.*, 2005, **38**, 2087–2094.

